JOURNAL OF SOLID STATE CHEMISTRY 114, 190–198 (1995)

Reflection High-Energy Electron Diffraction Monitored Growth of Infinite-Layer $SrCuO_2/CaCuO_2$ Thin Film Heterostructures

A. Gupta, T. M. Shaw, M. Y. Chern, B. W. Hussey, A. M. Guloy, and B. A. Scott

IBM Thomas J. Watson Research Center, Yorktown Heights, New York 10598-0218

Received February 2, 1994; in revised form May 16, 1994; accepted May 18, 1994

Reflection high-energy electron diffraction (RHEED) intensity oscillations have been used for controlled, layer-by-layer growth of thin film heterostructures of the infinite-layer end-member compounds $SrCuO_2$ and $CaCuO_2$. These artificially structured films are grown on (100) $SrTiO_3$ substrates by pulsed laser deposition under a low-pressure oxygen ambient, using a combination of atomic oxygen and pulsed molecular oxygen, at a relatively low temperature of 500°C. X-ray diffraction and transmission electron microscopy are used for the structural characterization of the epitaxial heterostructures. Systematic variations in the electrical properties of the multilayers have been observed as a function of the thickness of the $SrCuO_2$ and $CaCuO_2$ layers for unit-cell-level modulation periods. © 1995 Academic Press, Inc.

1. INTRODUCTION

Over the past few years, the pulsed laser deposition (PLD) technique has rapidly emerged as one of the simplest and most versatile methods for the deposition of thin films of a wide variety of materials (1). The stoichiometric removal of constituent species from the target during ablation, as well as the relatively small number of control parameters, makes the PLD technique particularly attractive for the synthesis of complex multicomponent phases such as the high T_c cuprate superconductors. The PLD technique has recently been extended to the fabrication of epitaxial heterostructures and superlattices of various cuprates, both for use in device applications and for the investigation of the fundamental properties of high-temperature superconductors (2). By allowing the films to grow in a two-dimensional (2D) layer-by-layer mode, with thickness control down to the unit cell level, the technique further offers the possibility of artificially fabricating a wide variety of metastable cuprate structures which would be difficult or impossible to synthesize by conventional bulk methods. This includes potentially new superconducting cuprates with higher transition temperatures than have been attained thus far.

For the deposition of artificially structured films with compositionally abrupt interfaces, it is important to monitor the surface structure and to precisely control the growth of individual layers, using *in situ* analysis techniques such as reflection high-energy electron diffraction (RHEED). It has generally been observed for PLD growth that, in order to obtain films with good superconducting properties, a relatively high background pressure of oxygen is necessary during deposition (3). This is particularly true for the growth of complex oxide structures such as $YBa_2Cu_3O_{7-\delta}$, where the formation of defect phases, which are nonsuperconducting or which have depressed T_c's is usually favored at O_2 pressures far below 100 mTorr. The need to operate at high background pressures, however, severely restricts the *in situ* operation of the RHEED, due to both electron scattering and oxidation of the electron-gun filament.

To circumvent the above process limitations for *in situ* RHEED monitoring, we have developed a novel low-pressure PLD technique in which a pulsed source is used to supply a high instantaneous flux of oxygen for the oxidation of the ablated cation species arriving at the substrate (4). Additionally, an atomic oxygen source is provided for the thermodynamic stability of the films at the growth temperature. Because of the relatively low background pressure (≤1 mTorr) maintained during deposition, *in situ* characterization of the surface using RHEED can be readily accomplished. The pressure in the region of the RHEED gun filament is further reduced by differential pumping and is about three orders of magnitude lower than the pressure in the main chamber.

The RHEED-monitored PLD system has recently been used for the layer-by-layer growth of thin films of the infinite-layer end-member compounds, $SrCuO_2$ (SCO) and $CaCuO_2$ (CCO) (5). The infinite-layer parent structure of the cuprate superconductors is one of the simplest systems containing CuO_2 layers (6). These layer units form an important structural component of a number of known cuprate superconductors and can possibly be used as building blocks for the tailored synthesis of new, metastable cuprate structures. In addition, appropriate doping of the infinite-layer compounds themselves can render them metallic and lead to superconductivity (7, 8). Inter-

0022-4596/95 $6.00

estingly, the infinite-layer compounds exhibit superconductivity with both n-type doping for T_c's of ~40 K (7) and p-type doping for T_c's up to 110 K (8). Hiroi *et al.* (8) have observed bulk p-type superconductivity, with T_c up to 110 K, in the cation-deficient infinite-layer $Ca_{1-x}Sr_xCuO_2$ compounds prepared at high pressures. The superconducting phase in this system has, however, not yet been positively identified. Resistive and magnetic anomalies at temperatures as high as 180 K have also been reported by Li *et al.* (9) in thin films of this system grown by laser MBE. The magnitudes of the resistivity drop and the diamagnetic signal observed in the thin films are, however, extremely small, suggesting that the fraction of any possible superconducting phase present in the samples is negligible. Clearly, since the stoichiometric $Ca_{1-x}Sr_xCuO_2$ phases with a formal copper valence of Cu^{2+} are antiferromagnetic insulators, some method of chemical substitution or nonstoichiometry is required for doping which will result in superconductivity in these compounds. A likely method for hole-doping of the CuO_2 planes involves creation of alkaline-earth-deficient defect layers in the infinite-layer structure (8). Hole-doping can also possibly be achieved by monovalent ion (Na^+, Li^+, etc.) substitution or by the introduction of excess oxygen into the structure.

It is well known that cation ordering plays a crucial role in a large number of known superconducting cuprates. Thus, it seems reasonable to assume that cation ordering may also be important for inducing superconductivity in the $Ca_{1-x}Sr_xCuO_2$ compounds. Doping of these ordered phases can perhaps be controlled by the specific insertion of excess oxygen in the layers containing the larger Sr^{2+} ions, whose ionic radii is appropriate for 12-fold coordination with oxygen. Complete oxygenation around the Sr ions would then result in the formation of an ordered structure, partially consisting of copper–oxygen square pyramids stacked through sharing their apical oxygen.

With the above structural perspective for oxygen doping, we have synthesized a number of the infinite-layer-related films, with ordered stacking of the isostructural Sr- and Ca-containing layers, using the PLD layer-by-layer growth technique. Besides the possibility of superconductivity, these artificially structured infinite-layer films also provide a model system to study the microstructural details and compositional integrity of the individual layer units in cuprate heterostructures. We have been able to synthesize heterostructures of the SCO and CCO infinite-layer compounds with a relatively high degree of structural perfection and ordering of the cations. The electrical properties of these films have been observed to be quite sensitive to the oxygen annealing conditions, with films cooled in the presence of atomic oxygen exhibiting relatively low resistivities. Furthermore, systematic variations in the resistive properties of the films have been observed as a function of the modulation periods of the Sr and Ca ions on a unit-cell scale. However, under our process conditions, we have not found any indication of superconductivity in any of these ordered structures.

2. EXPERIMENTAL

The basic experimental setup for the RHEED-monitored pulsed laser deposition system has been described in detail previously (4). Briefly, a focused KrF excimer laser (248 nm) is used for ablation, with pulse energy of ~40 mJ and a fluence of 2–3 J/cm^2 at the target. The films are deposited on optically polished (100)-oriented $SrTiO_3$ substrates, which are glued with silver paint to a stainless steel heater block to ensure good thermal contact. The heater block can be rotated and translated for the proper positioning of the azimuth and incidence angles for RHEED measurements. A pulsed source of O_2 is directed at the substrate during deposition using an electromagnetically operated pulsed valve; the opening of the valve and the triggering of the laser are synchronized with an appropriate delay to ensure that the gas jet and the ablated fragments arrive at the substrate at the same time. In addition to the pulsed O_2, a continuous flux of atomic O, produced downstream by the microwave dissociation of O_2 in a McCarrol cavity, is also flowed near the substrate through a quartz tube. The quartz tube is pretreated with boric acid to suppress the wall-recombination rate of the atomic oxygen produced in the discharge. The atomic O flux at the substrate position has been found to be in the range 1–2 $\times$ 10^{16} atoms/cm^2 as measured with a silver-coated quartz monitor. With the pulsed valve operating at 2–4 Hz, the background pressure in the growth chamber is maintained at ~1 mTorr during deposition.

The Sr and Ca cuprate targets used for ablation are prepared by compacting and reacting mixtures of the appropriate precursor nitrates of 900°C in air. This preparative route does not produce the infinite-layer phase, and the Sr cuprate target has been determined by X-ray analysis to consist predominantly of the stable $SrCuO_2$ orthorhombic phase, whereas the Ca target is observed to be a homogeneous mixture of the Ca_2CuO_3 and CuO compounds.

Before deposition of the heterostructures, the (100) $SrTiO_3$ substrates are heated to 650–700°C, and the surface was cleaned using a 150-eV Ar-ion beam. This is followed by homoepitaxial deposition of $SrTiO_3$, from a single-crystal $SrTiO_3$ target, until a bright and streaky RHEED spectra, with a well-developed pattern of Kikuchi lines, is obtained. With additional growth of Sr TiO_3, strong intensity oscillations of the specular spot are

observed due to the 2D layer-by-layer growth of the deposit (10). The growth of the buffer layer ensures a very smooth substrate surface, which is essential for subsequent layer-by-layer growth and the observation of RHEED oscillations during deposition of the cuprate layers.

Growth of the $SrCuO_2/CaCuO_2$ (SCO/CCO) multilayer films is normally initiated after deposition of a 10–20-nm-thick buffer layer of $SrTiO_3$. Before growth of the heterostructures, a few monolayers of SCO are deposited first and their growth rate is accurately determined from the period of the RHEED oscillations (corresponding to the growth of a monolayer of SCO of unit-cell thickness (5)). This is followed by the deposition of a few monolayers of CCO, and its growth rate is similarly obtained from the observed RHEED oscillations. Having calibrated the deposition rates of the individual infinite-layer compounds, the number of laser pulses used for ablation from each target is programmed for automated deposition of a periodically repeated sequence of n unit cells of SCO and m unit cells of CCO, with a growth interruption of 30–60 sec in between the layers to allow time for surface recovery. Thus, a multilayered film of 1×2 periodicity refers to the periodic stacking of one unit cell of SCO and two unit cells of CCO. The two layers define one cycle, and the cycle is repeated a number of times to increase the film thickness.

With a few specific exceptions, all the multilayer films have been grown at a substrate temperature of 500°C, with a deposition rate of ~0.01 nm/pulse and a total film thickness in the range 50–100 nm. Following deposition, the films are slowly cooled to room temperature either in the presence of atomic O (maintaining the same concentration as used during growth), or after backfilling the chamber with 760 Torr O_2. Some of the films have also been postannealed at temperatures of 200–400°C in a high-pressure oxygen vessel pressurized to 400 bar. At higher pressures and temperatures the films are observed to decompose quite readily.

The cation stoichiometry of the single-layer SCO and CCO films were checked using Rutherford backscattering spectroscopy (RBS) and were found to be within 5% of the nominal target composition. The oxygen composition of the films has, however, not been determined, and it is likely that they are not always stoichiometric in oxygen, particularly when the films are cooled in atomic oxygen. High-resolution X-ray diffraction in the normal Bragg-reflection and grazing-incidence modes using CuKα radiation, and cross sectional TEM are used for structural characterization of the films. Samples for electron microscopy have been prepared by conventional cross section TEM techniques and are thinned to electron transparency by ion-beam milling with a 3-keV Argon-ion beam. Four-probe dc transport measurement has been used for electrical characterization of the films, for which they are patterned using a laser-microscope system (248 nm), with a fluence of ~1 J/cm^2, to form 50–100-μm-wide and 200-μm long microbridges.

3. RESULTS AND DISCUSSION

The epitaxial growth of SCO thin films on lattice-matched $SrTiO_3$ substrates has been previously reported by a number of investigators (11, 12). On the other hand, it has been difficult to obtain epitaxial films of the other end-member, CCO. We have recently demonstrated that films of the infinite-layer CCO phase can be readily stabilized by using an intermediate layer of infinite-layer SCO film as a chemical template for its nucleation and growth (5). To explain the growth of the highly metastable CCO phase, we have suggested that the terminating CuO_2 layer of SCO possibly acts as a "seed" for the nucleation and replication of the infinite-layer structure during the deposition of the precursor atoms. Because of the relatively low growth temperature (500°C), the SCO and CCO films can also be deposited without atomic O, in a low pressure O_2 ambient (~1 mTorr). However, the presence of atomic O has been found to promote the 2D growth of these compounds.

The growth of the SCO/CCO multilayers is initiated after the growth of a few monolayers of the SCO template. We have observed that, irrespective of the thickness of the individual layers, the RHEED pattern during the deposition of the SCO/CCO multilayers remains sharp and streaky. The RHEED patterns observed during the growth cycle of a film of 1×1 stacking periodicity, at the end of the deposition of the CCO and SCO layers, are shown in Fig. 1. In addition to a streaky RHEED pattern, the associated Kikuchi lines are also observed in Fig. 1, suggesting that growth surface remains atomically smooth during the 2D layer-by-layer growth of the film.

The layer-by-layer growth also results in intensity oscillations of the spots of the zero-order Laue zone during the deposition of each compound (5). While these oscillations are damped quite rapidly, they can be reinitiated if the growth is interrupted for a brief period during which the intensity recovers to its original value. We have previously reported that for the infinite-layer compounds the growth unit corresponding to the period of the intensity oscillations is a single unit cell (5). The monolayer growth thickness corresponds to the minimum unit of the structure which is needed to satisfy the chemical composition and electrical neutrality criteria (13). The intensity oscillations observed during the growth of a film of 1×1 periodicity, using an automated sequence of depositing a monolayer and then interrupting the growth for 30 sec to allow time for surface recovery, are shown in Fig. 2.

We have characterized the multilayer structures in the

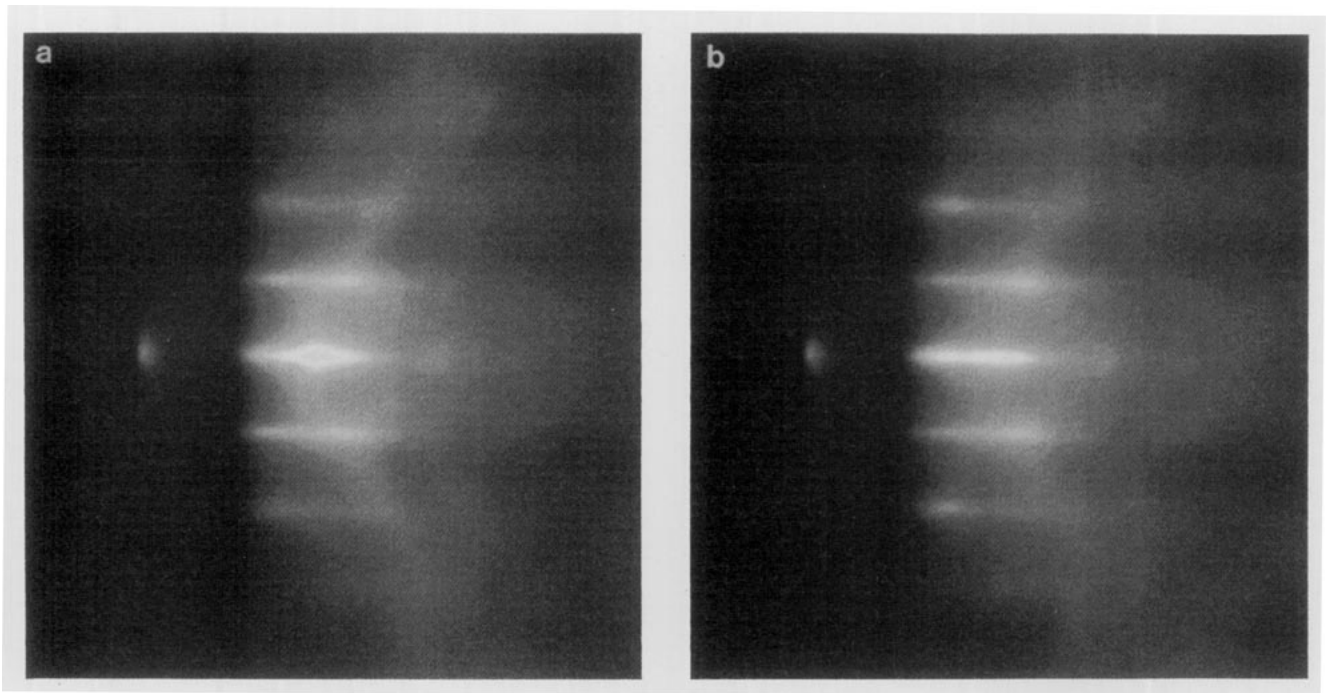

FIG. 1. RHEED patterns observed during the deposition cycle of a multilayer $SrCuO_2/CaCuO_2$ film of 1 × 1 stacking periodicity (a) at the end of deposition of $CaCuO_2$ layer and (b) after deposition of the $SrCuO_2$ layer. Beam azimuth, [100]; beam energy, 10 keV.

direction normal to the interface using X-ray diffraction in the Bragg-reflection geometry. The X-ray scans in the range of the first- and second-order diffraction peaks for single-layer SCO and CCO films, and four multilayer SCO/CCO films with different stacking periodicities are shown in Fig. 3. The simulated patterns for these films, calculated using a commercially available software program based on dynamic theory (14), are shown below the experimental patterns. The diffraction peaks for the SCO and CCO films shown in Fig. 3 can be indexed as the first- and second-order reflections of the infinite-layer phase with the c-axis oriented normal to the plane of the substrate. The lattice parameters for the CCO and SCO films are determined to be 0.318 nm and 0.345 nm, respectively. A small increase in the c-axis parameter of both the CCO (0.321 nm) and SCO (0.347 nm) films have been

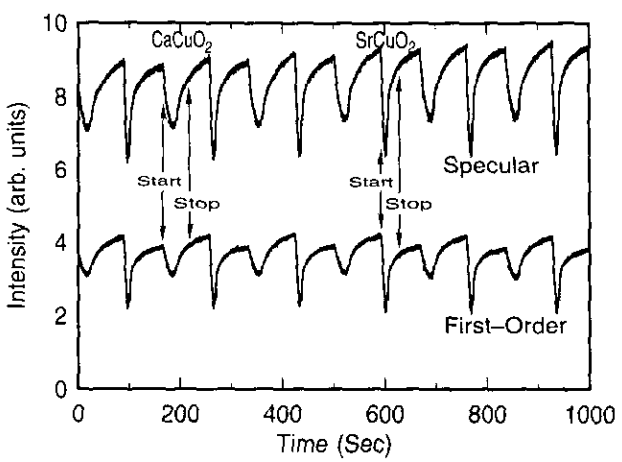

FIG. 2. Intensity oscillations of the specular and first-order diffracted spots in the RHEED pattern during growth of a 1 × 1 multilayer $SrCuO_2/CaCuO_2$ film with a 30-sec recovery period between the deposition of successive layers.

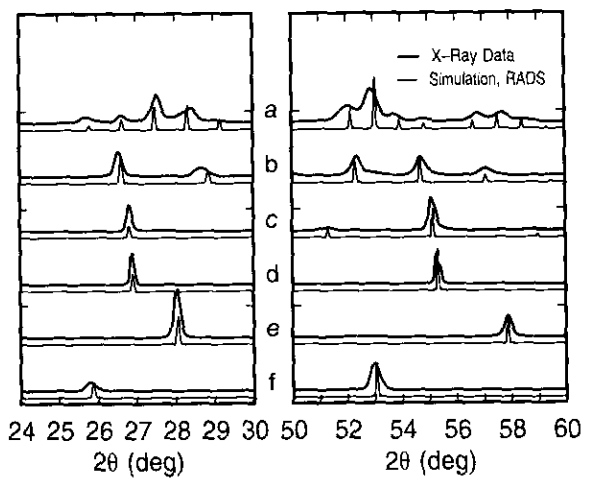

FIG. 3. X-ray diffraction θ–2θ scans in the range of the first- and second-order peaks for $CaCuO_2$ (CCO) and $SrCuO_2$ (SCO) and four multilayer SCO/CCO firms with different stacking periodicities: (a) 20 × 12 SCO/CCO, (b) 8 × 4 SCO/CCO, (c) 4 × 4 SCO/CCO; (d) 1 × 1 SCO/CCO, (e) CCO, and (f) SCO films. All the films have been cooled under 760 Torr O_2. The calculated patterns are shown below each scan.

observed when they are cooled in atomic O instead of O_2 (5).

The multilayer films in Fig. 3 show characteristic satellite peaks resulting from the modulation of the Sr and Ca containing sites. Note that there is reasonably good agreement between the calculated and measured peak positions and relative intensities for all the multilayer films, suggesting that the actual stacking periodicities for the multilayers are in close agreement with the programmed values. Nonetheless, the experimentally observed peak widths are in general significantly broader than the calculated peak widths. This is primarily because the calculation does not account for the effects of strain in the layers, or the presence of dislocations and other structural defects, which will result in peak broadening. Moreover, interfacial disorder or intermixing may be partly responsible for the observed differences between the calculated and measured spectra.

In addition to the X-ray scans in the normal Bragg-reflection geometry, some of the multilayer films have also been examined in directions parallel to the interface using grazing-incidence X-ray diffraction (15). The scans show that the films are epitaxially oriented with in-plane lattice constants $a = b \simeq 0.39$ nm for both the SCO and CCO layers, which is essentially identical to the lattice parameters of the $SrTiO_3$ substrate within experimental resolution. In the bulk, the reported values for the in-plane lattice parameters are 0.392 nm for SCO and 0.385 nm for CCO (from extrapolation of the values for $Ca_{0.86}Sr_{0.14}CuO_2$ and $SrCuO_2$). Thus, the in-plane coherency is expected to result in strain in the perpendicular c-axis direction which is compressive for the SCO films and tensile for the CCO layers. This will lead to a slight contraction of the c-axis for the CCO layers and expansion for the SCO layers compared to their relaxed values.

Figure 4 shows a portion of a low-magnification cross-

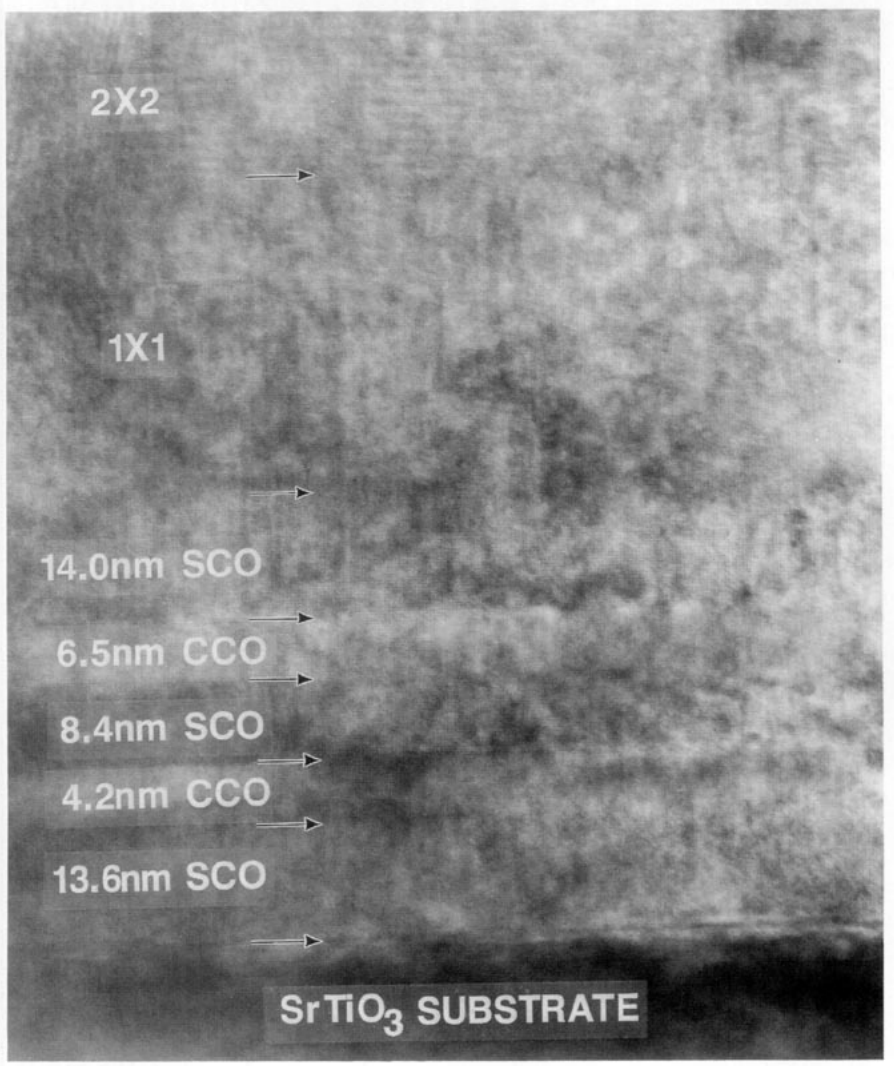

FIG. 4. Low-magnification cross sectional TEM image of a $SrCuO_2/CaCuO_2$ multilayer structure grown on a (100) $SrTiO_3$ substrate.

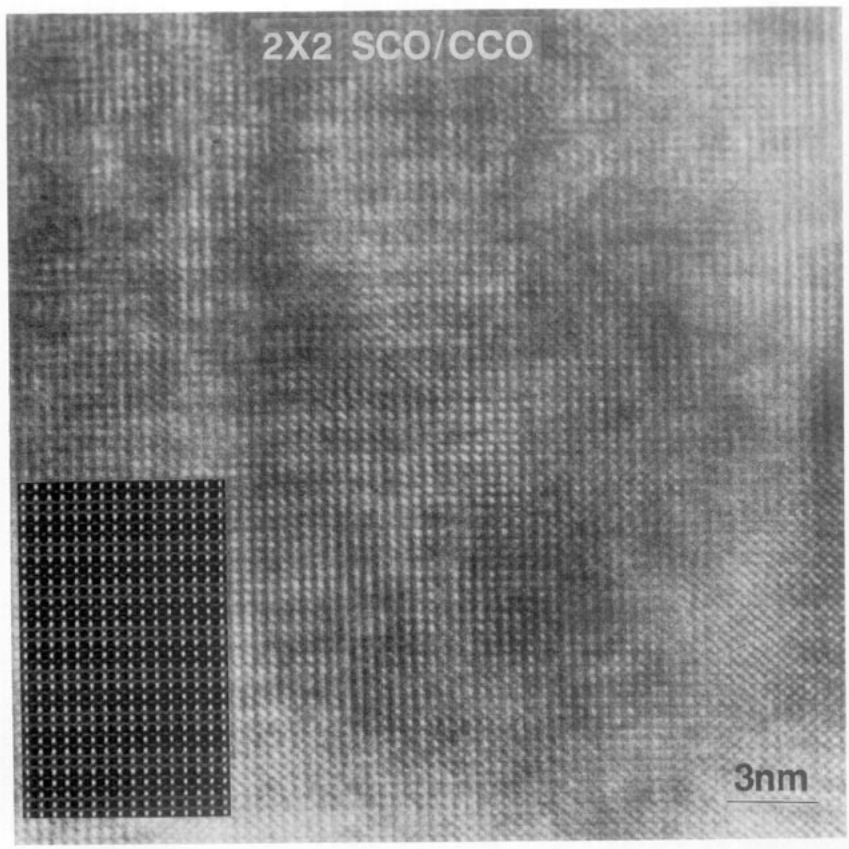

FIG. 5. High-resolution transmission electron image of the 2 × 2 $SrCuO_2/CaCuO_2$ superlattice structure taken with the incident electron beam along the [010] direction. Faint modulation in contrast with a four-unit-cell repeat distance can be observed in the image. The inset shows an image simulation of a perfect 2 × 2 superlattice in a 10-nm-thick specimen at Scherzer defocus.

sectional TEM image of a multilayer film containing different thickness layers of SCO and CCO, which were specifically grown for electron microscopy observations. The bottom of the figure corresponds to the $SrTiO_3$ substrate used for the deposition and above it are alternating layers of SCO and CCO. From the slight layer-to-layer variations in contrast, an accurate measurement of the thickness of the different layers can be made. The measured thicknesses and the layer sequence confirm that the RHEED oscillation periods correspond to the deposition of unit cell layers of the two compounds.

In the top portion of the figure, layers in which an attempt to deposit 1 × 1 and 2 × 2 superlattices of the two structures are shown. A faint contrast modulation is evident in the superlattice 2 × 2 layer and indicates that some modulation in the Sr/Ca concentration is present in this layer. The contrast modulation is seen more clearly in the high-resolution image of the 2 × 2 superlattice (Fig. 5). Here a distinct but faint modulation in contrast with a four-unit-cell repeat distance can be seen. Simulations of the high resolution images of the 2 × 2 superlattice show that only slight differences in contrast between the SCO and CCO layers should be present even when no intermixing has occurred between the layers. An example for a 10-nm-thick specimen imaged at the Scherzer defocus is shown inset in Fig. 5. The fact that there is an observable, although faint, contrast between the layers suggests that quite a strong composition modulation is present in the 2 × 2 superlattice layer of the deposit.

A selected area diffraction pattern from the film is shown in Fig. 6. The pattern confirms that the film is epitaxially aligned with the substrate. In the horizontal (h00) row of reflections, the reflections from the (100) planes of the SCO and CCO layers superimpose on the (100) reflection of the substrate indicating that the film is epitaxially well matched to the substrate. Observation of higher order reflections, however, shows that the lattice constant of the film is slightly smaller than that of the substrate, which indicates that the film has partially lost coherency with the substrate. The vertical row of reflections corresponds to the (001) planes of the structures which are aligned parallel to the plane of the substrate. The first weaker reflection arises from the $SrTiO_3$ substrate. Above it is a triplet of reflections that arise from

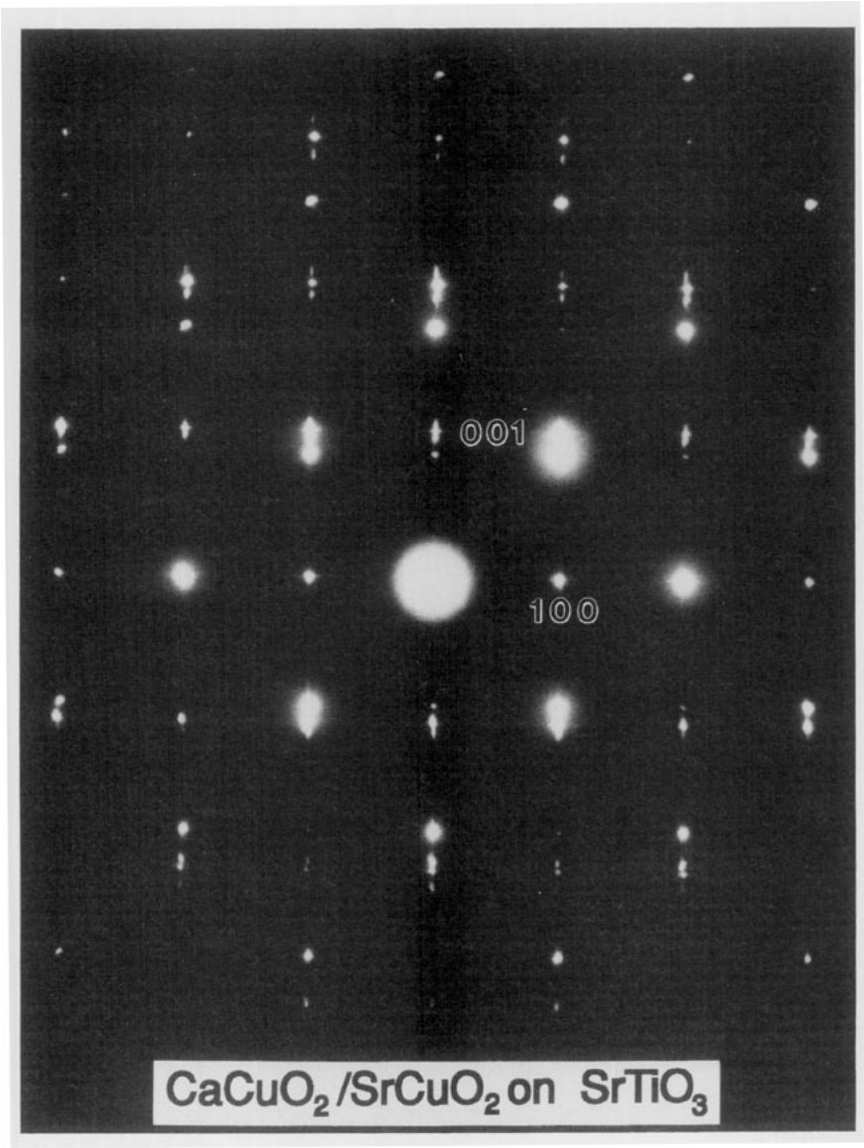

FIG. 6. Selected area diffraction pattern from the multilayer structure shown in Fig. 4 grown on a (100) $SrTiO_3$ substrate.

the film. Measurements, calibrated using the $SrTiO_3$ reflections, indicate that the reflections correspond to d spacings of 0.317, 0.333, and 0.345 nm. The larger d spacing agrees well with that expected for SCO and the smaller with that of CCO. The intermediate spacing arises from the superlattice portions of the film.

In addition to the diffraction spots, faint streaks along the [100] direction appear in the diffraction pattern. These arise from planar defects on the (100) planes of the SCO and CCO structures. Figure 7 shows a high resolution image of the defects. The origin of the defects is unclear. However, no displacement of the cation lattice seems to be associated with the defects as has been reported for other planar defects observed in $SrCuO_2$ thin films (16). It is possible that the defects are associated with ordered arrangements of oxygen vacancies.

The temperature dependence of the resistivity for various SCO/CCO multilayer films deposited at 500°C and then cooled in atomic O are displayed in Fig. 8. The resistivity plots for single-layer SCO and CCO films, prepared under the same conditions, are also shown for comparison. Interestingly, when the films were cooled in O_2 they were all highly resistive. As seen in Fig. 8, the SCO film cooled in atomic O has a relatively low room-temperature resistivity ($\sim 5 \times 10^{-3}$ Ω cm) and exhibits a semimetallic behavior as a function of temperature. On the other hand, we have observed that when the film is cooled in 760 Torr O_2 it is at least two orders of magni-

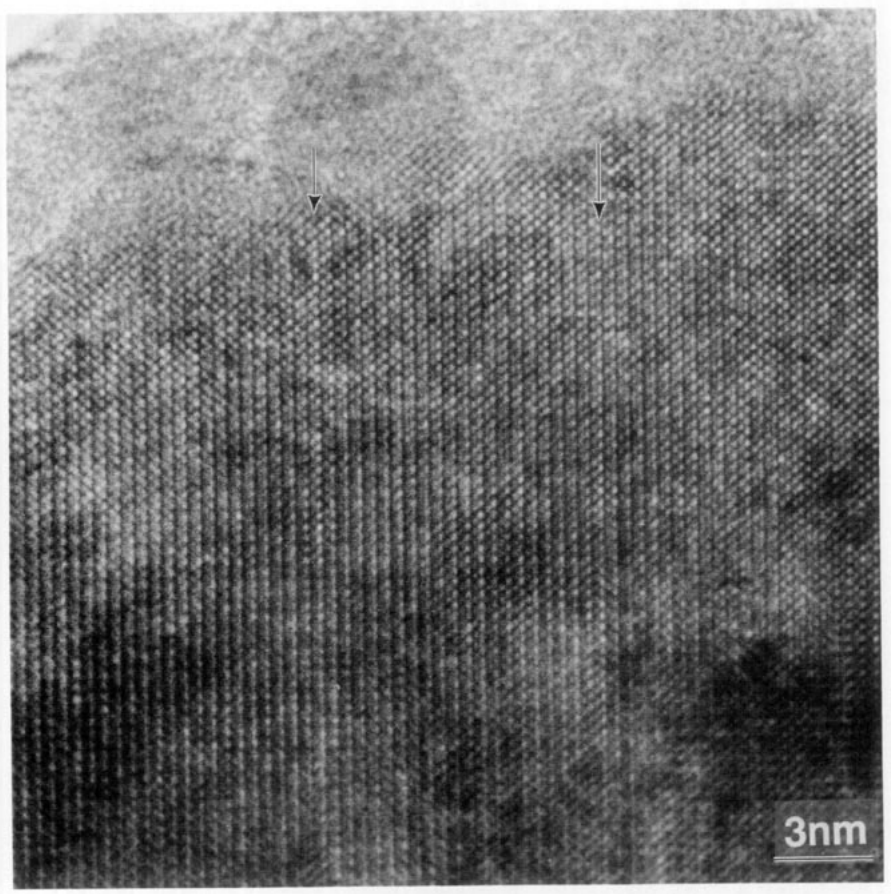

FIG. 7. High-resolution transmission electron image of a portion of the multilayer structure showing the planar defects (marked by arrows) on the (100) planes.

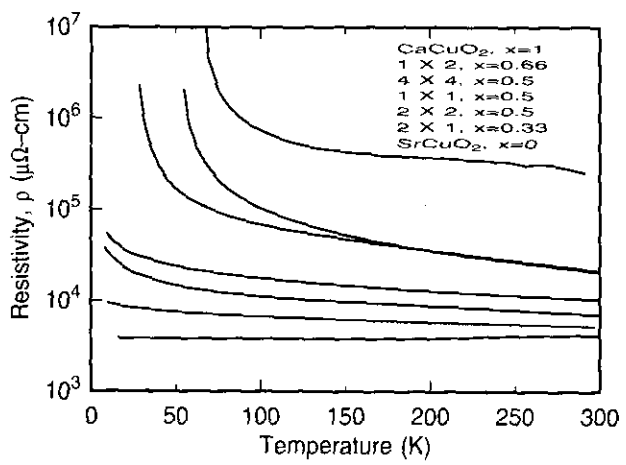

FIG. 8. Resistivity vs temperature of single-layer SCO and CCO films and of several multilayer SCO/CCO films with different stacking periodicities (listed top to bottom in the order shown in the figure). All the films were grown at 500°C under the same oxidation conditions and subsequently cooled in atomic oxygen.

tude more resistive and displays insulting characteristics (5). The wide variations in the resistivity of SCO as a function of oxygen concentration are possibly caused by lattice defects or imperfections. It is likely that excess oxygen is introduced in the Sr layer when the films are cooled in the presence of atomic O (film oxygen stoichiometry $2 + \delta$). This is supported by preliminary Hall measurements which indicate that the carriers are primarily holes. Unlike the SCO films, the resistance characteristics of the CCO films, containing the smaller alkaline earth cation, are much less sensitive to the ambient oxygen used during the cooldown cycle. Independent of the oxygen concentration, the $CaCuO_2$ films are highly resistive with only slight variations in their resistivity values. Furthermore, no changes are observed when the films are annealed at 200–300°C under high oxygen pressure.

It is observed in Fig. 8 that the resistivities for the SCO/CCO multilayer films fall between those of the single-layer SCO and CCO films. Moreover, the resistivity increases as the average ratio of Ca/Sr in the film in-

creases. The results are qualitatively consistent with the behavior expected for a parallel resistive network of SCO and CCO layers, although the details cannot be explained based solely on this model. This suggests that the interaction between the different layers is sufficiently weak and does not significantly influence the transport properties. It should be mentioned that some level of intermixing between the layers will also result in a progressive increase in the film resistivity with increasing Ca concentration, and may be partly responsible for the observed behavior. However, it is difficult to explain on this basis alone the resistivity values for the 1×2, 2×2, and 4×4 multilayer films, which have the same average concentration of Ca. We finally note that no evidence of superconductivity has been observed down to 5 K in any of the multilayer $SrCuO_2/CaCuO_2$ films we have studied.

ACKNOWLEDGMENTS

We thank G. Coleman for the RBS analysis and J. Angilello for the X-ray diffraction studies of the films.

REFERENCES

1. For example, see D. C. Paine and J. C. Bravman (Eds). "*Laser Ablation for Materials Synthesis*" Materials Research Society, Pittsburgh, PA. 1990.
2. H. Tabata, T. Kawai, and S. Kawai, *Phys. Rev. Lett.* **70,** 2633 (1993); A. Gupta, R. Gross, E. Olsson, A. Segmüller, G. Koren, and C. C. Tsuei, *Phys. Rev. Lett.* **64,** 3191 (1990); Q. Li, X. X. Xi, X. D. Wu, A. Inam, S. Vadlamannati, W. L. McLean, T. Venkatesan, R. Ramesh, D. M. Hwang, J. A. Martinez, and L. Nazar, *Phys. Rev. Lett.* **64,** 3086 (1990).
3. A. Gupta, B. W. Hussey, and M. Y. Chern, *Physica C* **200,** 263 (1992).
4. M. Y. Chern, A. Gupta, and B. W. Hussey, *Appl. Phys. Lett.* **60,** 3046 (1992).
5. A. Gupta, B. W. Hussey, T. M. Shaw, A. M. Guloy, M. Y. Chern, R. F. Saraf, and B. A. Scott, *J. Sol. State Chem.* **112,** 113 (1994).
6. M. Takano, Y. Takeda, H. Okada, M. Miyamoto, and K. Kusaka, *Physica C* **159,** 375 (1989); T. Siegrist, S. M. Zahurak, D. W. Murphy, and R. S. Roth, *Nature* **334,** 231 (1988).
7. N. Ikeda, Z. Hiroi, M. Azuma, M. Takano, Y. Bando, and Y. Takeda, *Physica C* **210,** 367 (1993); G. Er, Y. Miyamoto, F. Kanamaru, and S. Kikkawa, *Physica C* **181,** 206 (1991); M. G. Smith, A. Manthiram, J. Zhou, J. B. Goodenough, and J. T. Markert, *Nature* **351,** 549 (1991).
8. Z. Hiroi, M. Azuma, M. Takano, and Y. Takeda, *Physica C* **208,** 286 (1993); M. Azuma, Z. Hiroi, M. Takano, Y. Bando, and Y. Takeda, *Nature* **356,** 775 (1992); M. Takano, M. Azuma, Z. Hiroi, Y. Bando, and Y. Takeda, *Physica C* **176,** 441 (1991).
9. X. Li, T. Kawai, and S. Kawai, *Jpn. J. Appl. Phys.* **31,** 934L (1992).
10. M. Y. Chern, A. Gupta, B. W. Hussey, and T. M. Shaw, *J. Vac. Sci. Technol. A* **11,** 637 (1993).
11. D. P. Norton, B. C. Chakoumakos, J. D. Budai, and D. H. Lowndes, *Appl. Phys. Lett.* **62,** 1679 (1993); C. Niu and C. M. Lieber, *J. Am. Chem. Soc.* **114,** 3570 (1992); X. Li, M. Kanai, T. Kawai, and S. Kawai, *Jpn. J. Appl. Phys.* **31,** L217 (1992).
12. Y. Terashima, R. Sato, S. Takeno, S. Nakamura, and T. Miura, *Jpn. J. Appl. Phys.* **32,** L48 (1993); N. Sugii, M. Ichikawa, K. Kubo, T. Sakurai, K. Yamamoto, and H. Yamauchi, *Physica C* **196,** 129 (1992).
13. T. Terashima, Y, Bando, K. Iijima, K. Yamamoto, K. Hirata, K. Hayashi, K. Kamigaki, and H. Terauchi, *Phys. Rev. Lett.* **65,** 2684 (1990).
14. Rocking Curve Analysis by Dynamic Simulation (RADS), Bede Scientific Instruments Ltd., Bowburn, Durham, UK.
15. A. Segmüller, *Thin Solid Films* **18,** 287 (1973).
16. N. Sugii, M. Ichikawa, K. Hayashi, K. Kubo, K. Yamamoto, and H. Yamauchi, *Physica C* **213,** 345 (1993); S. Takeno, S. Nakamura, Y. Terashima, and T. Miura, *Physica C* **206,** 75 (1993).